Bio-Inspired Synergistic Model Predictive Control for Control Reallocation and Reduced Computational Cost in a Hybrid Exoskeleton

Krysten Lambeth, Noor Hakam, and Nitin Sharma*

***Abstract*—Dynamic optimization is a versatile control tool to determine optimal control inputs in a redundantly actuated wearable robot. However, dynamic optimization requires high computational resources for real-time implementation. In this paper, we present a bio-inspired control approach, based on the principle of muscle synergies, to reduce the computational cost of optimization. The most important linear combinations of actuators, dubbed "artificial synergies," were identified for the double support phase (DSP) and single support phase (SSP) of walking, allowing for hip, knee, and ankle actuation. In simulations, we compared the bio-inspired (input dimensionality reduced) model predictive control (MPC) with a conventional MPC using the full-dimensional actuation model. For both the DSP and SSP, incorporating synergies reduces the mean number of iterations per optimization step. A minimum number of synergies are indeed necessary to truly achieve redistribution of control effort across the other actuators when a primary muscle is fatigued. Additionally, we provide a practical approach to conduct real-time experiments with the bio-inspired MPC. A data-driven modeling approach is used to identify the nonlinear musculoskeletal dynamics and extract personalized artificial synergies from the experimental hybrid exoskeleton walking data. Synergistic MPC reduces computation time by an average of 28.16% ($p < 0.03$) compared to full-dimensional MPC. Furthermore, we demonstrate control redistribution in response to varying cost function penalties on individual synergy activations. It is, to the authors' knowledge, the first instance of artificial synergy-based MPC in real-time for a hybrid gait exoskeleton. This study provides insight into the use of bio-inspiration for hybrid exoskeleton control and other rehabilitation systems with redundant actuators.**

***Index Terms*—Hybrid Neuroprostheses, Muscle Synergies, Dimensionality Reduction, Functional Electrical Stimulation, Powered Exoskeleton, Gait Assistance, Model Predictive Control**

I. Introduction

Assistive lower-limb exoskeletons such as the Indego and ReWalk use motorized hip and knee joints [1], [2] to provide gait assistance for people with spinal cord injury, multiple sclerosis, and other neurological conditions [3]–[5]. These powered exoskeletons can be augmented with functional electrical stimulation (FES), which has been previously shown to aid in walking by coordinating desired muscle contractions in dorsiflexors, plantar flexors, quadriceps, hamstrings, and gluteals [6]–[8].

K. Lambeth, N. Hakam, and N. Sharma are with the UNC/NC State Lampe Joint Department of Biomedical Engineering, NC State University, Raleigh, NC 27606 USA (e-mail: {kflambet, nzhakam, nsharm23}@ncsu.edu).

*Corresponding author: Nitin Sharma. This work was funded by NSF SCH Award #2124017.

The resulting human-exoskeleton system, also known as a hybrid exoskeleton, becomes actuator redundant. A range of control techniques have been developed for the hybrid exoskeleton [9]–[11]. "Muscle-first" strategies supplement open-loop FES with feedforward exoskeleton assistance [12], while cooperative approaches have used feedback control for the exoskeleton while adapting FES profiles based on joint trajectory error [13]. Such approaches address exoskeleton and FES control separately, however, limiting the ability of the exoskeleton to compensate for FES-induced muscle fatigue progression, which remains a major technical challenge for the clinical adoption of FES as an assistive technology. In this paper, we focus on an optimal control-based multi-joint control allocation strategy to redistribute input as the FES-induced muscle fatigue sets in.

Model predictive control (MPC) for high-degree-of-freedom hybrid exoskeletons either incorporates feedback linearization or linearizes the model along the trajectory [14]–[16]. Although this approach neglects the nonlinearity of a multi-link model (due to inertial and Coriolis terms and nonlinear stimulation input-muscle force mappings), linearization facilitates a large number of iterations per optimization step for real-time implementation. There exists a need for a control method which optimally coordinates FES and exoskeleton motors across multiple degrees of freedom without the need for model linearization or feedback linearization. Moreover, existing MPC techniques are not formulated to compensate for fatigue effects in a major force-producing muscle, such as the ankle plantar flexors, across multiple joints. Optimal control has indeed been pursued for fatigue compensation during single-joint control of hybrid exoskeletons [17], but not across multiple joints.

Bio-inspired techniques offer a means of simplifying an optimal control scheme for a multi-joint hybrid exoskeleton and making real-time implementation of a nonlinear MPC (NMPC) possible. For this technique to become favorable, we use the principle of muscle synergies [18], [19] for bioinspiration. The muscle synergy hypothesis posits that the human spinal cord uses a library of coactivations to produce complex motions. These synergies can be identified by performing non-negative matrix factorization on EMG signals collected across multiple muscles. Different synergies can be associated with different motions, such as the commonly accepted sequence of synergies used during walking, namely, push off, foot clearance, leg deceleration, and weight acceptance. Push off is dominated by plantar flexor activity, weight acceptance by

quadriceps activity, and so forth [20]–[22]. Mainly, synergies are hypothesized as a way for the human motor control system to deliver limb movements in a computationally efficient manner [19]. In our past work on a hybrid exoskeleton [23]–[26], we showed that if only a few linear combinations of control inputs are dominant, input dimensionality can be reduced by using the most important linear combinations to elicit stepping-like movements. In this bio-inspired approach, the deduced actuator weights, referred to as "artificial synergies," facilitate input dimensionality reduction, allowing the stepping movement via a feedback control law comprised of a few synergy coefficients. However, the bio-inspired framework has not been extended in an optimal control framework where an NMPC can exploit these artificial synergies to reduce computational cost.

The main contributions of this paper are the comparisons of an NMPC using bioinspiration with a conventional NMPC. Using simulations and experiments, we show that the bio-inspired NMPC is particularly useful in reducing computational cost, vis-à-vis a full-dimensional MPC. We compare the average number of iterations per optimization step and the average objective function value across control cases and fatigue conditions. Simulations depict fatigue compensation using various numbers of synergies in both the double support and single support phases of walking. Importantly, we provide a practical approach to conduct real-time experiments with the bio-inspired MPC that uses personalized artificial synergies, extracted from an available set of viable experimental control input data. Moreover, we use a data-driven approach to identify the nonlinear musculoskeletal walking dynamics from the experimental hybrid exoskeleton walking data. The data-driven model is then employed in the bio-inspired MPC to validate its advantageous over full-dimensional MPC.

The paper is structured in the following sections: Section II describes a 4-link hybrid neuroprosthesis gait model with realistic control inputs. Section III-A provides an NMPC approach to extract synergies via principal component analysis (PCA), and Section III-B shows a subsequent NMPC approach to determine synergy activations (control inputs) to produce stepping movements. The results on computational costs and control effort distribution in response to muscle fatigue are discussed in Section IV. Section V details the procedures for identifying person-specific synergies from hybrid exoskeleton walking data and how synergistic MPC was implemented in real-time. The experimental results are presented in Section VI. Finally, Section VII discusses the simulation and experimental findings, and a conclusion is provided in Section VIII.

II. Musculoskeletal Models

Remark 1. For simplicity, we refer to the ankle plantar flexors and dorsiflexors as the ankle extensors and flexors, respectively. This is consistent with the terminology in [27], from which we derive the active and passive muscle torque relations subsequently described. A detailed derivation of the dynamics without the inclusion of the swing foot can be found in [28], but we present an overview here.

A. Single Support Phase Model

The single support phase (SSP) model consists of a stance leg, swing thigh, swing shank, and swing foot segments. The 4-link musculoskeletal dynamics is given as

$$M_s(q_s)\ddot{q}_s = C_s(q_s, \dot{q}_s)\dot{q}_s + G_s(q_s) + \tau_s(t), \tag{1}$$

where $q_s, \dot{q}_s, \ddot{q}_s \in \mathbb{R}^4$ are the angles, angular velocities, and angular accelerations of the limb segments with respect to the vertical, visualized in Fig. 1(a). Specifically, the limb segment angle vector is given as $q_s = [q_{st}, q_t, q_s, q_f]$, where q_{st}, q_t, q_s, $q_f \in \mathbb{R}$ are the angles of the stance leg, swing thigh, swing shank, and swing foot. The terms $M_s, C_s \in \mathbb{R}^{4\times4}$, $G_s \in \mathbb{R}^4$ are the mass matrix, Coriolis matrix, and gravitational torque vector, respectively, for the SSP. Henceforth, subscript $j = [e, f]$ represents the extensor and flexor muscles groups.

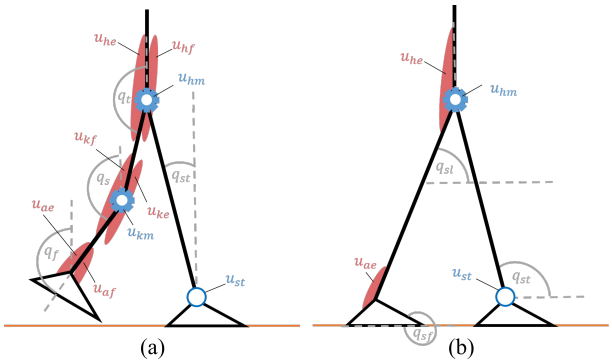

Fig. 1. Model diagrams for (a) the SSP and (b) the DSP. Angle definitions: q_{st} = stance leg, q_t = swing thigh (SSP), q_s = swing shank (SSP), q_f = swing foot (SSP), q_{sl} = swing leg (DSP), q_{sf} = swing foot (DSP).

The torque $\tau_s \in \mathbb{R}^4$ during the SSP contains motor torques, FES-elicited muscle torques, and a lumped torque acting at the stance ankle in addition to passive viscoelastic torques. For practical implementation, this torque can be considered a sum of the stance hip motor torque, FES-elicited stance ankle extensor torque, and the torque exerted by the user on a walker or similar assistive device. In terms of individual joint torques, the active torque can be broken down as [28]

$$\tau_s = \begin{bmatrix} -\Gamma_{st} + \Gamma_h \\ \Gamma_h - \Gamma_k \\ \Gamma_k - \Gamma_a \\ \Gamma_a \end{bmatrix}, \tag{2}$$

where Γ_i is the torque at joint i and $i = [st, h, k, a]$ represents the stance ankle, swing hip, swing knee, and swing ankle joint, respectively. The anatomical joint angles $q_h, q_k, q_a \in \mathbb{R}$ are related to the limb segment angles as

$$\begin{aligned} q_h &= q_t - \pi \\ q_k &= q_t - q_s \\ q_a &= q_f - q_s. \end{aligned}$$

The joint torques in (2) are written as

$$\begin{aligned}\Gamma_{st} &= M_{st}u_{st} \\ \Gamma_h &= \kappa_1 u_{hm} - \psi_{he}\mu_{he}u_{he} + \psi_{hf}\mu_{hf}u_{hf} - F_{hp} \\ \Gamma_k &= \kappa_2 u_{km} + \psi_{ke}\mu_{ke}u_{ke} - \psi_{kf}\mu_{kf}u_{kf} + F_{kp} \\ \Gamma_a &= -\psi_{ae}\mu_{ae}u_{ae} + \psi_{af}\mu_{af}u_{af} - F_{ap},\end{aligned} \tag{3}$$

where control inputs $u_{st}, u_{hm}, u_{km} \in [-1, 1]$ are the normalized stance leg, hip motor, and knee motor torques, which are respectively multiplied by maximum torque values $M_{st}, \kappa_1, \kappa_2 \in \mathbb{R}^+$. The FES inputs u_{ij}, $i = [h, k, a]$, $j = [e, f]$ are normalized with respect to subject-specific threshold and saturation currents and are bounded as $u_{ij} \in [0, 1]$. The control set $\mathbb{U}_{SSP} \subset \mathbb{R}^9$ is thus

$$\begin{aligned}\mathbb{U}_{SSP} := \Big\{ & u_{st}, u_{hm}, u_{km} \in [-1, 1] \\ & \cap u_{ij} \in [0, 1], i = [h, k, a], j = [e, f] \Big\}.\end{aligned} \tag{4}$$

The functions ψ_{ij}, $j = [e, f]$, $i = [h, k, a]$ in (3) contain muscle torque-length and torque-velocity terms and are given as

$$\begin{aligned}\psi_{if} &= \left(c_{if2}\varphi_i^2 + c_{if1}\varphi_i + c_{if0}\right)\left(1 - c_{if3}\dot{\varphi}_i\right) \\ \psi_{ie} &= \left(c_{ie2}\varphi_i^2 + c_{ie1}\varphi_i + c_{ie0}\right)\left(1 + c_{ie3}\dot{\varphi}_i\right),\end{aligned}$$

where $\varphi_i, \dot{\varphi}_i \in \mathbb{R}$ are the ith anatomical joint angle and angular velocity and $c_{ij0}, \ldots, c_{ij3} \in \mathbb{R}$ are person-specific parameters. The passive viscoelastic joint torques $F_{ip} \in \mathbb{R}$ in (3) are given as [29]

$$F_i = d_{i1}(\varphi_i - \varphi_{i_0}) + d_{i2}\dot{\varphi}_i + d_{i3}e^{d_{i4}\varphi_i} - d_{i5}e^{d_{i6}\varphi_i}$$

for $i = [h, k, a]$ and subject-specific parameters $d_{i1}, \ldots, d_{i6}, \varphi_{i_0} \in \mathbb{R}$, where φ_{i_0} is the angle at which the net torque at joint i is 0. The muscle efficiency index (MEI) $\mu_{ij} \in [\mu_{min_{ij}}, 1]$ quantifies the fatigued state of muscle ij. Specifically, a fully rested muscle, which can elicit the maximum possible torque, has $\mu_{ij} = 1$. As it fatigues, the muscle is able to produce less and less torque, and thus μ_{ij} decays. The MEIs are subject to their own dynamics [30], given as

$$\dot{\mu}_{ij} = \frac{(\mu_{min_{ij}} - \mu_{ij})}{T_{f_{ij}}}u_{ij} + \frac{(1 - \mu_{ij})}{T_{r_{ij}}}(1 - u_{ij}), \tag{5}$$

where $\mu_{min_{ij}} \in (0, 1)$ is the minimum MEI value and $T_{f_{ij}}, T_{r_{ij}} \in \mathbb{R}^+$ are fatigue and recovery time constants.

B. Double Support Phase Model

The double support phase (DSP) model consists of stance leg, swing leg, and swing foot segments as well as the ground between the stance and swing feet. Note that, for the DSP, "swing" leg/foot refers to the leg/foot which will *enter* the swing phase at the end of double support. The DSP is thus a closed-chain model [28] whose dynamics is given as

$$M_d\ddot{q}_{st} = C_d(q_{st}, \dot{q}_{st}) + G_d(q_{st}) + \tau_d, \tag{6}$$

where $M_d, C_d, G_d \in \mathbb{R}$ are the inertial, Coriolis, and gravitational torques during DSP and $q_{st} \in \mathbb{R}$ is the angle of the stance leg with respect to the horizontal by which the angles of the swing foot and swing leg (q_{sf} and q_{sl}, respectively) are parameterized. Angle definitions are visualized in Fig. 1(b). The torque during DSP $\tau_d \in \mathbb{R}$ is given by

$$\begin{aligned}\tau_d = M_{st}u_{st} + \kappa_1 u_{hm} + \psi_{he}\mu_{he}u_{he} \\ + \psi_{ae}\mu_{ae}u_{ae} + F_{hp} + F_{ap}.\end{aligned}$$

We do not consider the ankle flexors of the swing leg as ankle flexion would not contribute the push off required to propel the hip joint forward and enter the swing phase. Although the knee flexors and extensors both contribute during DSP in unassisted walking [31], our model does not consider any active or passive torques at the knee as we assume the joint to be mechanically locked during this phase. The control set $\mathbb{U}_{DSP} \subset \mathbb{R}^4$ is therefore

$$\mathbb{U}_{DSP} := \Big\{u_{st}, u_{hm} \in [-1, 1] \cap u_{he}, u_{ae} \in [0, 1]\Big\}. \tag{7}$$

III. Synergy Decomposition & Control Allocation

A. Synergy Decomposition

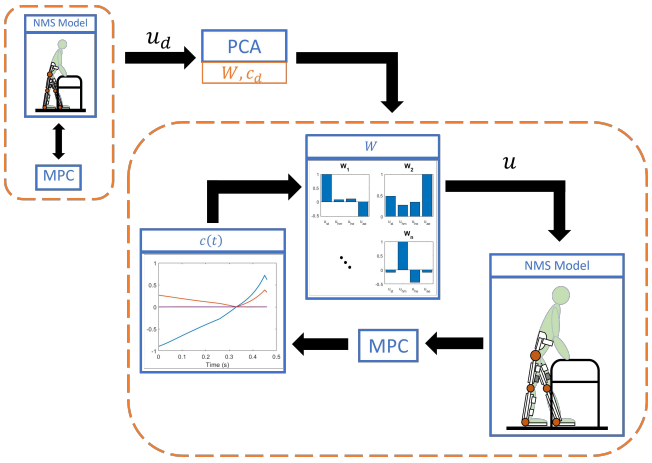

Fig. 2. High-level diagram of synergy extraction and simulations with MPC. For both gait phases, the optimal full-dimensional activations u_d are obtained using MPC with a neuromusculoskeletal model. Synergy weights W and corresponding synergy activations c_d are extracted from u_d through PCA. Using a truncated weight matrix to reduce input dimensionality, MPC then provides the optimal synergy activations c for the same neuromusculoskeletal model but with the inclusion of fatigue dynamics. Multiplying Wc yields the full-dimensional input u to the model.

Consider a vector of $m \in \mathbb{N}$ optimized control inputs across $k \in \mathbb{N}$ sampling instants, denoted $u_d \in \mathbb{R}^{m \times k}$. Linear algebraic methods such as principal component analysis (PCA) and non-negative matrix factorization can be applied to identify the $p \leq m$ most prevalent linear combinations of control inputs in u_d [19], [23]. Extracting the synergies allows us to write the controls as

$$u_d = Wc_d + u_{loss}, \tag{8}$$

where $W \in \mathbb{R}^{m \times p}$ is a matrix of constant synergy weights and $c_d(t) \in \mathbb{R}^{p \times k}$ contains the corresponding desired synergy activation signals. The j^{th} column of W, therefore, represents

a unique combination of control inputs, and the j^{th} row of c_d contains its corresponding time-varying activation.

The term $u_{loss} \in \mathbb{R}^m$ represents the reconstruction error, or the discrepancy between u_d and Wc_d. Choosing a greater number of synergies will decrease the magnitude of this reconstruction error, with the typical cutoff being 90% of the variance accounted for (VAF) [23].

To obtain u_d, simulations were run in MATLAB (R2020b, MathWorks, MA, USA) using the fast MPC operator CasADi [32]. Muscle parameters were within the experimental range for people with SCI [27], [29], and rigid-body parameters were obtained using anthropometric data from [33]. The model was prescribed a height of 1.8m and a weight of 80kg. The maximum hip and knee motor torques κ_1, κ_2 were chosen as 54 Nm, which is realistic for lower-body exoskeletons, and the maximum torque M_{st} exerted by the stance leg was chosen as 300 Nm. When M_{st} is divided by the moment arm, i.e., the length of the stance leg, the resultant force is well below the expected body weight of an adult and is therefore physically realistic.

The overall synergy extraction and simulation procedure is depicted in Fig. 2. The steps for this process are as follows:

1) For the given model (DSP or SSP), use MPC to determine the optimal full-dimensional control inputs u_d.
2) Implement PCA to extract synergy weights W and synergy activations c_d from u_d.
3) Truncate W to reduce input dimensionality.
4) To account for information loss, use MPC to identify the new optimal synergy activations c, incorporating fatigue dynamics into the model.

For both the DSP and SSP, the MPC was formulated as follows:

$$\min_{u_s(t|t_k)} \quad J^*\left(x_s(t|t_k), u_s(t|t_k)\right) = \int_{t_k}^{t_k+T} l_s \, dt \tag{9}$$

$$\dot{x}_s = f_s\left(x_s(t|t_k), u_s(t|t_k)\right) \tag{10}$$

$$u_s(t|t_k) \in \mathbb{U}_s, \tag{11}$$

where $s = [DSP, SSP]$, $x(t|t_k)$ is the prediction of future state $x(t)$, $t \in [t_k, t_k+T]$, at sampling instant t_k for prediction horizon duration $T \in \mathbb{R}^+$. The dynamics, derived from (6) and (1) for the DSP and SSP, respectively, are represented by (10) with $x_{DSP} = [q_{st}, q_{sf}, q_{sl}, \dot{q}_{st}]^T \in \mathbb{R}^4$ for the DSP and $x_{SSP} = [q_s^T, \dot{q}_s^T]^T \in \mathbb{R}^8$ for the SSP. The control bounds (11) for both phases are as defined in (4) and (7). The cost function l_s is given as

$$l_s\left(x_s(t|t_k), u_s(t|t_k)\right) = \|x_{d_s} - x_s\|^2_{Q_s} + \|u\|^2_{R_s}, \tag{12}$$

where $x_{d_{DSP}}(t) \in \mathbb{R}^4$, $x_{d_{SSP}}(t) \in \mathbb{R}^8$ are vectors of desired joint angles and angular velocities during the DSP and SSP, respectively, and $Q_{DSP} \in \mathbb{R}^{4\times4}$, $Q_{SSP} \in \mathbb{R}^{8\times8}$, $R_{DSP} \in \mathbb{R}^{4\times4}$, $R_{SSP} \in \mathbb{R}^{9\times9}$ are positive definite, diagonal weight matrices. The desired trajectories were obtained from [28].

While achieving sufficient forward velocity of the hip and completing a step are the main objectives during DSP and SSP, respectively, we penalized joint space error in the cost function to ensure that synergies were extracted from a smooth stepping trajectory. The alternative would have been to penalize the error between the task-space location of the endpoint (hip joint in DSP and toe in SSP) to a desired task-space trajectory. In simulation, this can result in a somewhat jerky trajectory. Since the goal was to extract synergies that achieved a smooth, coordinated motion, we found it most appropriate to penalize joint space error.

To decompose the synergies, we applied PCA. In contrast to non-negative matrix factorization, PCA allows the weights to be negative, which is appropriate given that the normalized stance leg torque and motor torques can be negative. Let c_j be the j^{th} element in activation vector c and W_{ij} be the element in row i, column j of W. Although the normalized FES inputs are non-negative, it is possible for the i^{th} reconstructed input

$$u_i = \sum_j W_{ij} c_j$$

to be negative because the individual synergy weights W_{ij} and activations c_j can be negative. This consideration will be addressed in Section III-B.

B. Control Allocation with Fatigue

Due to the information loss during synergy extraction, it may not be suitable to simply apply the reconstructed control inputs Wc_d as in (8). It is instead advisable to apply optimal or adaptive synergy-based control, obtaining a new set of synergy activations $c(t)$ but utilizing the same set of weights W. Therefore, following synergy extraction, simulations were carried out using synergistic MPC. While W is fixed, the MPC was free to choose new $c(t)$ profiles that differed from the $c_d(t)$ profiles obtained during the synergy extraction process. The MPC was formulated as

$$\begin{aligned} \min_{c_s(t|t_k)} \quad & J^*\left(x_s(t|t_k), c_s(t|t_k)\right) = \int_{t_k}^{t_k+T} l_s \, dt \\ & \dot{x}_s = f_s\left(x(t|t_k), W_s c_s(t|t_k)\right) \\ & c_s(t|t_k) \in \mathbb{U}_s, \end{aligned} \tag{13}$$

where W_s is the truncated constant synergy matrix for $s = [DSP, SSP]$. The control bounds $\mathbb{U}_s \in \mathbb{R}^p$ are defined as $\mathbb{U}_{DSP} := \{c \mid |c_j| \leq 7, \forall j\}$ and $\mathbb{U}_{SSP} := \{c \mid |c_j| \leq 0.7, \forall j\}$, where c_j is the j^{th} synergy activation. For each gait phase, we identified the muscle which received the greatest root-mean-square (RMS) optimal FES input. The MEI dynamics (5) of this muscle was then included in (13). The cost functions were defined as

$$\begin{aligned} l_{DSP}\left(x_{DSP}(t|t_k), c_{DSP}(t|t_k)\right) = & \left\| \begin{array}{c} z_d - z \\ \dot{z}_d - \dot{z} \end{array} \right\|^2_{Q_z} \\ & + Q_{\mu_{DSP}}\left(1 - \mu_{ae}\right)^2 + \|W_{DSP} c_{DSP}\|^2_{R_{DSP}}, \end{aligned} \tag{14}$$

$$\begin{aligned} l_{SSP}\left(x_{SSP}(t|t_k), c_{SSP}(t|t_k)\right) = & \left\| \; x_{d_{SSP}} - x_{SSP} \; \right\|^2_{Q_{SSP}} \\ & + Q_{\mu_{SSP}}\left(1 - \mu_{he}\right)^2 + \|W_{SSP} c_{SSP}\|^2_{R_{SSP}} \end{aligned}$$

where $z_d(t)$ is the desired Cartesian task-space position of the hip, obtained from $x_{d_{DSP}}$ in (9), with time derivative $\dot{z}_d(t) \in \mathbb{R}^2$. Likewise, z, $\dot{z} \in \mathbb{R}^2$ are the actual task-space position and velocity of the hip. The matrices R_s and Q_{SSP} are the same as those used in (12). Positive diagonal weight matrix

$Q_z \in \mathbb{R}^{4\times4}$ penalizes task-space error, while the constants $Q_{\mu_s} \in \mathbb{R}^+$penalize fatigue.

Of note, there is not a simple way to bound c to ensure that the full-dimensional inputs u are bounded. While one could place additional constraints on $Wc = u$, this would increase computational burden and defeat one of the main purposes of using synergistic controls. Instead, while the model for the MPC did not employ constraints on u, we performed saturation in simulation. For the DSP, all inputs were saturated. For the SSP, negative FES inputs were set to 0, but we purposefully chose a bound on c such that, for most simulations, each element of $|u|$ remained below 1. For two simulations, u_{ke} exceeded 1, and for one simulation, u_{km} became less than -1. These control inputs were saturated accordingly.

Simulations were run under three initial muscle fatigue conditions for target muscle j: fully rested ($\mu_j(t_0) = 1$), partially fatigued ($\mu_j(t_0) = 0.5$), and fully fatigued ($\mu_j(t_0) = \mu_{min_j} = 0.05$). Each initial fatigue condition was simulated without synergies (that is, with full-dimensional controls). For the DSP, each condition was also simulated with $p = \{1, 2\}$ synergies. For the SSP, simulations were carried out using $p = \{3, 4\}$ synergies.

IV. Simulation Results

A. Double Support Phase

1) Synergy Extraction: For the DSP, two synergies accounted for 100% of the variance, with the first synergy alone accounting for 95.65% of the variance. We denote the activation profiles of synergies 1 and 2 by $c_1(t)$, $c_2(t)$, respectively, and the columns of W corresponding to synergies 1 and 2 are similarly denoted W_1, W_2. The weights and optimal activations for these synergies can be seen in Fig. 3(a) and (b), respectively. The first synergy is dominated by the stance leg torque and, to a lesser extent, by FES of the ankle extensors. The second synergy primarily activates the ankle extensors, with lesser weights on all remaining inputs.

2) Control Allocation with Fatigue: As can be seen in Fig. 4(a), in the case of one synergy, the optimal synergy activation trajectory depends on the initial fatigue state of the ankle extensors. Specifically, the synergy activation becomes more negative at the start of the simulation when the ankle extensors are more fatigued. This results in the stance leg torque saturating for a longer duration during the first half of the simulation, as can be seen in Fig. 4(b). It also results in greater FES intensity for the ankle extensors, with saturation occurring in the fully fatigued case. Notably, because there is only 1 synergy, the MPC is forced to saturate u_{ae} regardless of the penalty on ankle extensor fatigue in (14).

We now consider the case of 2 synergies. Whereas 1 synergy forced the MPC to choose between completing the task and offloading ankle extensor effort, 2 synergies provides the opportunity to redistribute the activations. The shapes of the synergy activation trajectories $c_1(t)$ and $c_2(t)$ vary dramatically depending on the initial ankle extensor fatigue state. Consequently, when the ankle extensors are fully or even halfway fatigued, no FES is sent to the muscle group at all, and the hip motor provides the requisite torque instead.

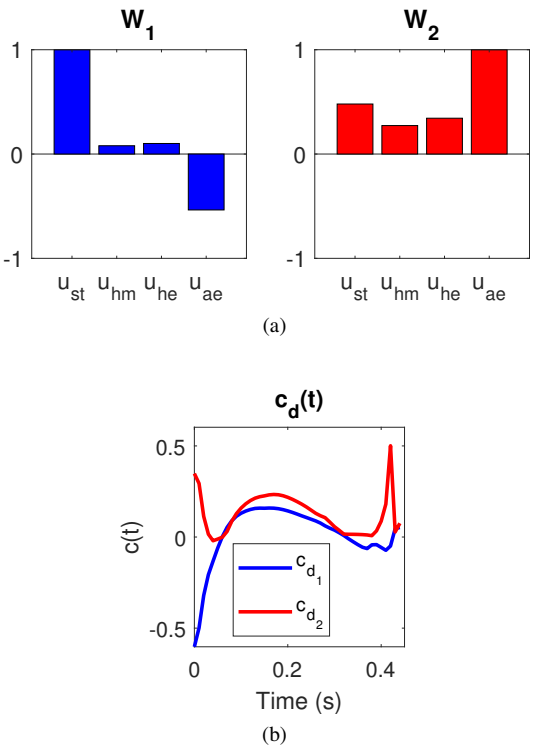

Fig. 3. (a) Weights and (b) optimal activations $c_d(t)$ for the two most dominant DSP synergies.

3) Computational Cost Reduction: Finally, we compare the computational burden and task-space trajectory tracking for the 1 synergy, 2 synergy, and full-dimensional cases. Quantitative performance metrics are reported in Table I, where FD denotes the full-dimensional case. For the case where $\mu_{ae}(t_0) = 1$, the 1 synergy and 2 synergy cases both carry out an average of 5.14 iterations per optimization step, while the full-dimensional case averages 12.30 iterations per step. This represents a 58.13% reduction, as seen in Fig. 5(a). For the fully fatigued and halfway fatigued conditions, the difference in computational cost between the 1 synergy and 2 synergy cases becomes more evident. The 1 synergy case reduces the number of iterations by 70.00% for the halfway fatigued condition and by 57.10% for the fully fatigued condition, whereas the 2 synergy case reduces the number of iterations by only 19.90% and 40.97%, respectively.

The impact of synergistic control on the mean value of the objective function depends on the initial fatigue condition. For the half-fatigued condition, the 1 synergy, 2 synergy, and full-dimensional cases have average cost function values of 250.71, 240.69, and 251.53, respectively. The 2 synergy case thus incurs a 4.00% lower cost, on average, while the 1 synergy case incurs an average cost less than 1% greater than the average full-dimensional cost, as Fig. 5(b) demonstrates. These percent differences are even smaller for the fully fatigued case. The magnitude of the mean cost function is less than 1 for the rested condition in each control case, making the large percent differences negligible in practice. The choice of initial fatigue value has a much greater effect on the cost function than the number of synergies, increasing it by orders of magnitude.

Control Case	Fatigue Condition	Mean # Iterations	Mean $J^*(x,u)$	x-RMSE (cm)	y-RMSE (cm)
FD	Rested	12.30	0.90	0.23	0.03
	Half-Fatigued	13.26	250.71	0.73	0.11
	Fully Fatigued	13.19	899.61	2.56	0.38
$p = 2$	Rested	5.15	0.29	0.22	0.03
	Half-Fatigued	10.62	240.69	1.57	0.13
	Fully Fatigued	7.79	892.40	1.01	0.15
$p = 1$	Rested	5.15	0.30	0.22	0.03
	Half-Fatigued	5.17	251.53	0.40	0.06
	Fully Fatigued	5.66	900.81	1.65	0.25

TABLE I
PERFORMANCE METRICS FOR THE DSP.

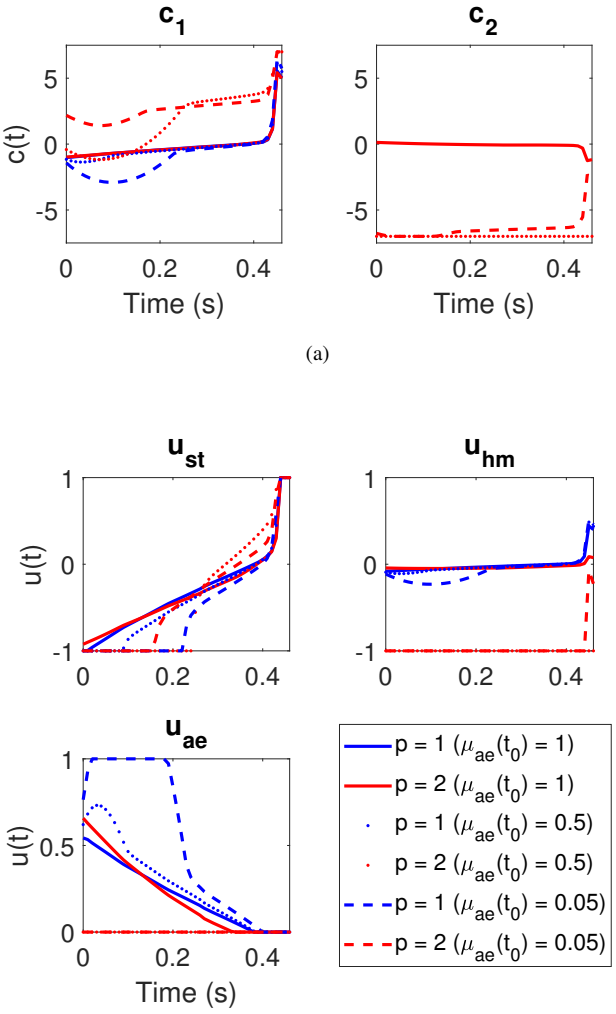

Fig. 4. Comparison of the 1-dimensional and 2-dimensional (a) DSP synergy activations and (b) stance leg, hip motor, and ankle extensor FES inputs across three ankle extensor fatigue conditions.

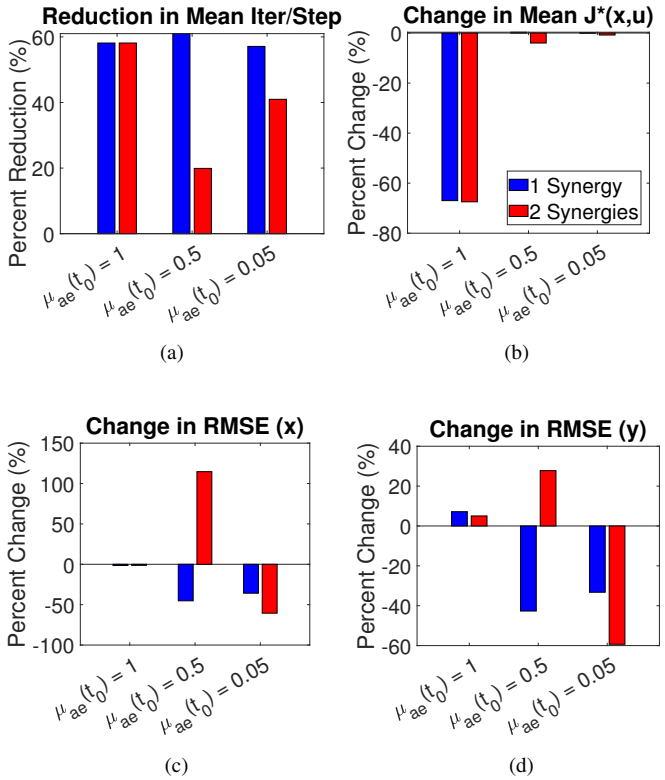

Fig. 5. (a) Percent reduction in mean number of iterations per optimization step for the DSP with 2 synergies, and 1 synergy, across ankle extensor fatigue conditions. (b) Percent change in average objective function value across control cases and fatigue conditions. (c) Percent change in task-space RMSE in the x-direction across control cases and fatigue conditions. (d) Percent change in task-space RMSE in the y-direction across control cases and fatigue conditions.

Lastly, in the x-direction, the difference in root-mean-square error (RMSE) of the hip compared to the full-dimensional case is less than 1 cm for the 2 synergy case and less than 2 cm for the 1 synergy case for all fatigue conditions. In the y-direction, the difference in hip RMSE between the full-dimensional and both synergistic cases is less than 1 cm for all fatigue conditions. Thus, while the percent changes shown in Fig. 5(c)-(d) appear sizable, the loss of information due to input dimensionality reduction has little impact on task performance.

B. Single Support Phase

1) Synergy Extraction: For the SSP, four synergies accounted for 99.22% of the variance, with three synergies explaining 95.68% of the variance. The first, second, third, and fourth synergies comprised 69.60%, 15.01%, 11.07%, and 3.54% VAF, respectively. As seen in Fig. 6(a), for a positive synergy activation signal, the first and second synergies provide hip flexion, but they differ in that the first synergy provides knee flexion (as indicated by the negative weight on

u_{km}) while the second synergy provides knee extension. The ankle muscles, especially the ankle extensors, have relatively small weights across the first four synergies, indicating low levels of activity for these muscles. The corresponding optimal activation profiles $c_d(t)$ can be seen in Fig. 6(b). The optimal RMS FES input was greatest for the hip flexors, so this muscle was initialized to different fatigue values in the next step.

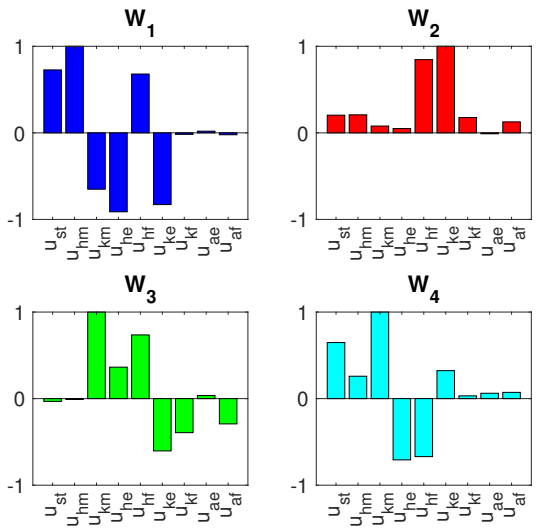

(a)

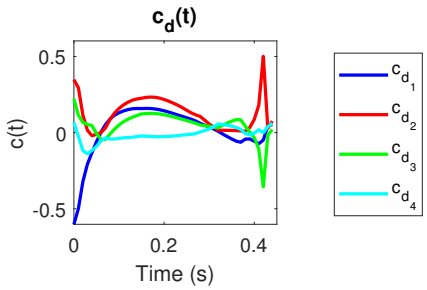

(b)

Fig. 6. (a) Weights and (b) optimal activations $c_d(t)$ for the four most dominant SSP synergies.

2) Control Allocation with Fatigue: Frames from the simulation with 3 synergies under the fully fatigued condition are presented in Fig. 7. Synergy strategies are presented in Fig. 8(a) and corresponding control inputs in Fig. 8(b) (note that, for brevity, we only included plots only for u_{st}, u_{hm}, and u_{hf}). The full-dimensional case responds to moderate hip flexor fatigue by increasing the FES dosage to the hip flexors, while in the fully fatigued case, the FES dosage is decreased. In both the partially and fully fatigued conditions, the full-dimensional case increases the stance leg and hip motor effort. By contrast, the 3 synergy case responds to greater hip flexor fatigue by increasing hip flexor FES. Like the full-dimensional case, the 3 synergy case increases the hip motor and stance leg effort, but the increase in hip motor effort is not as dramatic as in the full-dimensional case.

The 4 synergy case sees a reversal in fatigue compensation strategy. Specifically, while the hip flexor FES dosage remains

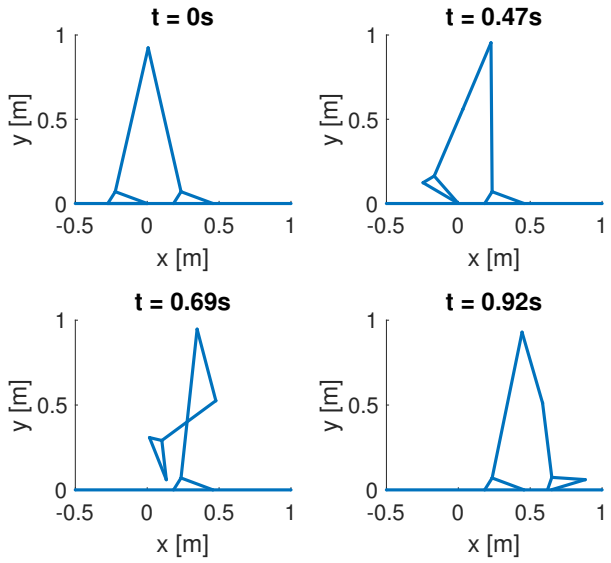

Fig. 7. The model taking a step. The top left figure shows the beginning of the DSP (simulation duration: 0.47s). The remaining three figures show the SSP model taking a step under the fully fatigued condition with 3 synergies (simulation duration: 0.45s). The total step time is therefore 0.92s.

relatively the same for the halfway fatigued case, for the fully fatigued case, the dosage is reduced. Again, the MPC opts to increase the hip motor torque and stance leg torque, increasing the stance leg torque by a greater amount than in the 3 synergy case.

3) Computational Cost Reduction: Quantitative performance metrics are reported in Table II. A comparison of the average number of iterations per optimization step across control cases reveals results that using 3-4 synergies reduces the mean number of iterations, although there is little difference in computational cost between the synergistic cases. The full-dimensional case carries out an average of more than 8 iterations per optimization step regardless of fatigue condition, and this is reduced to less than 6.9 iterations per step across all fatigue conditions with 4 synergies and less than 6.7 iterations per step with only 3 synergies. Fig. 9(a) shows the improvements in mean number of iterations.

Notably, despite the increased speed, the objective function value is less optimal for both synergistic cases than for the full-dimensional case, regardless of fatigue condition. Specifically, the mean objective function value is an order of magnitude greater for both synergistic cases than for the full-dimensional case regardless of fatigue condition, Fig. 9(b) illustrates. This may be due to information loss during the synergy extraction step.

Finally, as can be seen in Fig. 9(c) and (d), the synergistic cases have task-space RMSEs in the x- and y-directions that are greater than the task-space RMSEs for the full-dimensional case. The magnitudes of these differences are less than 5 cm in the x-direction and less than 3 cm in the y-direction for all control cases. While the cost function penalized joint-space error, the task-space trajectory is functionally significant because it determines the degree of foot clearance. Increases

Control Case	Fatigue Condition	Mean # Iterations	Mean $J^*(x,u)$	x-RMSE (cm)	y-RMSE (cm)
FD	Rested	8.45	43.79	1.76	1.11
	Half-Fatigued	8.64	50.66	1.42	1.07
	Fully Fatigued	10.45	10.62	1.22	0.98
$p=4$	Rested	6.07	122.88	3.78	1.74
	Half-Fatigued	6.29	179.81	4.40	2.26
	Fully Fatigued	6.89	167.45	5.54	3.06
$p=3$	Rested	6.49	168.31	4.94	1.45
	Half-Fatigued	6.51	171.22	4.36	1.56
	Fully Fatigued	6.62	163.58	4.29	2.27

TABLE II
PERFORMANCE METRICS FOR THE SSP.

in joint-space error are therefore not especially concerning as long as the model is able to take a step.

V. EXOSKELETON-ASSISTED WALKING EXPERIMENTS

A. Synergy Identification

This study was approved by the Institutional Review Board (IRB approval #: 20553; date: 12/10/2024) of North Carolina State University. One participant with SCI (injury level: T10; age: 56; weight: 113kg; sex: M), labeled S1, and two participants with no disabilities, labeled B1 (age: 21; weight: 75kg; sex: F) and B2 (age: 24; weight: 77kg; sex: F), provided informed consent and completed the experiments. To identify synergies as well as person-specific models for the MPC, each participant first walked in an Indego exoskeleton (Ekso Bionics, San Rafael, CA, USA) under a conventional feedback control scheme. We chose a PID controller to track predefined desired knee and hip angle trajectories. The exoskeleton is actuated by bilateral hip and knee motors, and ankle-foot orthoses have been modified to permit ankle motion. FES was applied to the quadriceps, hamstrings, dorsiflexors, and plantar flexors of both legs. The experimental setup is depicted in Fig. 10.

The exoskeleton was controlled via MATLAB (2024b) Simulink Desktop Real-Time (MathWorks, Natick, MA, USA). Position-based PID control was used for the motors, quadriceps FES, and hamstrings FES, but because the ankle joint was not instrumented with an inertial measurement unit, closed-loop ankle FES control could not be provided. Instead, we applied FES in open-loop for the ankle joint. A finite state machine determines the desired trajectories of the hip and knee joints, and each gait cycle is 9s in duration. Walking is initiated with a right half-step, followed by a rest phase and a full left step. The finite state machine then proceeds to alternate between 3.5s-duration right and left steps, with 1s rest phases between each step.

Participants walked on an instrumented split-belt treadmill (Bertec Corporation, Columbus, OH, USA) for 2 minutes while kinematic data was captured using Vicon Nexus software (Vicon Motion Systems Ltd, Los Angeles,CA, USA). Actual ankle joint trajectories were extracted from the motion capture data, while the exoskeleton recorded hip and knee joint trajectories. Finally, for each participant, synergies were extracted via PCA from all 6 control inputs (from the PID controller) for one leg (see (19)). The control input and kinematic output data was used to generate a person-specific model. Instead of identifying a nonlinear model as in (1) and (6), we used a Koopman-based data-driven approach [34], [35] to determine a linear model (in lifted space) of the SSP and DSP together (see Appendix for details). To avoid switched control, gait was not divided into stance and swing phases for model or synergy identification, and synergies were extracted across the gait cycle. The threshold for the minimum number of synergies was set at 90% VAF, which resulted in truncation to 3 synergies for all participants. These synergies are visualized in Fig. 11, and Table III lists the percentage of the data explained by each synergy.

Subject	Percentage Explained (%)		
	W_1	W_2	W_3
SCI	74.33	15.45	5.54
B1	70.83	14.04	8.95
B2	50.51	31.12	13.21

TABLE III
PERCENTAGES EXPLAINED BY EACH SYNERGY.

B. Real-Time Experiments with Synergy-Based MPC

Following model identification and synergy extraction, the MPC for synergistic control of the right leg of the hybrid exoskeleton was formulated as follows:

$$\min_{c(t|t_k)} \quad J^*\left(z(t|t_k), c(t|t_k)\right) = \int_{t_k}^{t_k+T} l\, dt \tag{15}$$

$$z(t|t_{k+1}) = Az(t|t_k) + BWc(t|t_k), \quad t \in [t_k, T] \tag{16}$$

$$c(t|t_k) \in \mathbb{U} := \{c \in \mathbb{R}^3 \mid |c_j| \leq 2, \forall j\}, \quad t \in [t_k, T]$$

where t_k is the initial time and $T \in \mathbb{R}^+$ is the length of the prediction horizon. The lifted state $z \in \mathbb{R}^{\mathcal{H}}$ (detailed in the Appendix) is of dimension $\mathcal{H} > 6$, where $x = [q^T, \dot{q}^T]^T \in \mathbb{R}^6$ contains the joint angles and angular velocities of the hip, knee, and ankle of the right leg. The allowed control set $\mathbb{U}$ was determined heuristically based on the magnitudes of the average synergy activation trajectories obtained during the synergy identification experiments. The cost function was given as

$$l\left(z(t|t_k), c(t|t_k)\right) = \|z - z_d\|_Q + \|c\|_R + \|\dot{c}\|_P, \tag{17}$$

where $Q \in \mathbb{R}^{\mathcal{H}\times\mathcal{H}}$, $R, P \in \mathbb{R}^{3\times3}$ are diagonal weight matrices and $\dot{c} \in \mathbb{R}^3$ is the time derivative of the synergy activation vector. The first 6 elements in z are simply x, while the remaining are nonlinear functions of the state. We therefore chose to make only the first 6 diagonal elements in Q nonzero.

An inbuilt MPC object in MATLAB was used to solve the optimal control problem for the right leg in real time.

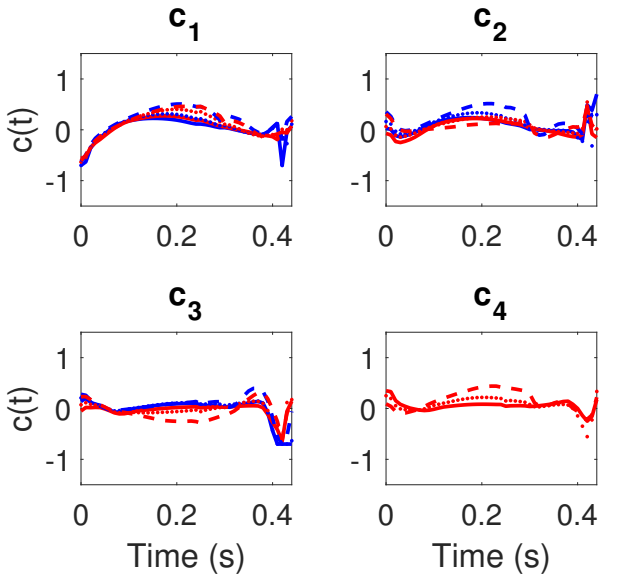

(a)

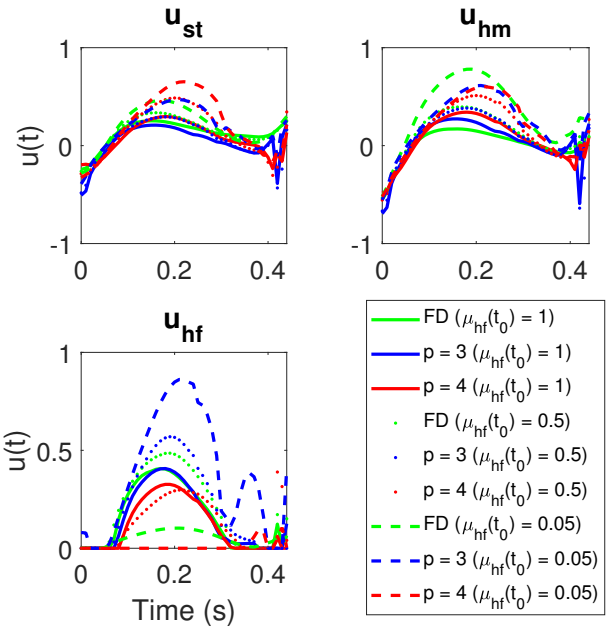

(b)

Fig. 8. Comparison of (a) the 3-dimensional and 4-dimensional SSP synergy activations and (b) the stance leg, hip motor, and hip flexor FES inputs across three hip flexor fatigue conditions. FD denotes the full-dimensional, non-synergistic case.

Control for the left leg was the same as that for synergy identification experiments. Each participant performed a 1-minute treadmill walking trial at a speed of ~0.05-0.12m/s, depending on participant step length. Desired hip and knee joint trajectories were the same as those used in the synergy identification experiments. Desired ankle trajectories were designed by averaging the ankle joint trajectories obtained from the participants with no disabilities during the synergy identification experiments. Because the ankle joint was not

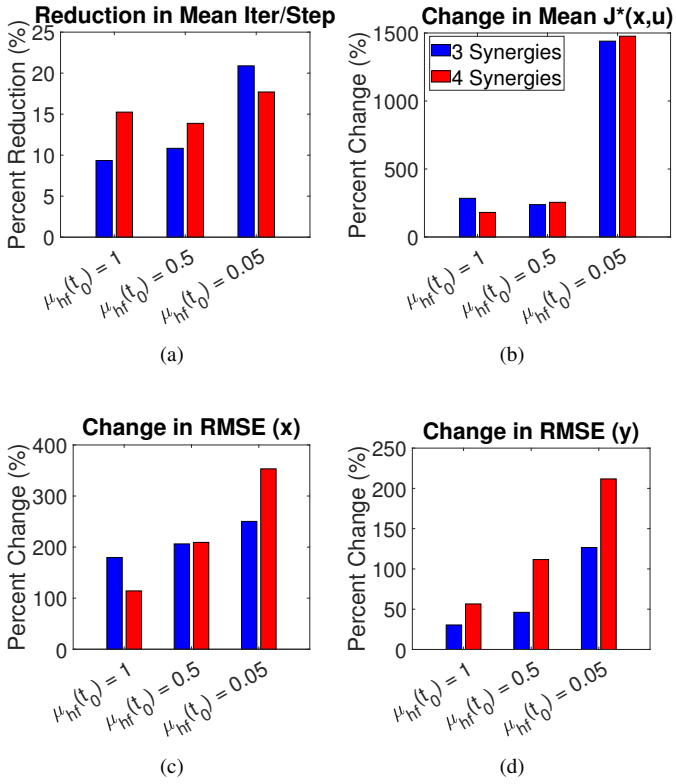

(a) (b) (c) (d)

Fig. 9. Comparison of (a) average number of iterations per optimization step and (b) average optimal cost function value with 3-4 synergies and with no synergies, across fatigue conditions, for the SSP. Comparison of RMSEs in the (c) x-direction and (d) y-direction across fatigue conditions for the SSP.

instrumented, the ankle trajectory could not be used as real-time feedback. Instead, a false ankle joint trajectory, defined as the desired trajectory delayed by 0.2s, was supplied as state feedback for the MPC.

Participants walked under the following conditions:

1) **Synergistic (Lower-Dimensional Bio-Inspired) MPC**. The personalized discrete-time dynamics in (16) is converted to continuous time via MATLAB's state-space model function, and BW is used as the control matrix. As in the simulations, the MPC selects the optimal synergy activation signals $c(t)$.
2) **Non-Synergistic MPC (Full-Dimensional).** For the non-synergistic case, the optimal control problem in (15) is replaced by

$$\begin{aligned} \min_{u(t|t_k)} \quad & J^*\left(z(t|t_k), u(t|t_k)\right) = \int_{t_k}^{t_k+T} l\, dt \qquad (18) \\ & z(t|t_{k+1}) = Az(t|t_k) + Bu(t|t_k), \quad t \in [t_k, T] \\ & u(t|t_k) \in \mathbb{U}, \quad t \in [t_k, T] \end{aligned}$$

where the control set $\mathbb{U} \subset \mathbb{R}^6$ is given as

$$\mathbb{U} := \begin{cases} u_j \in [-1, 1], & j < 3, \\ u_j \in [0, 1], & j \geq 3, \end{cases}$$

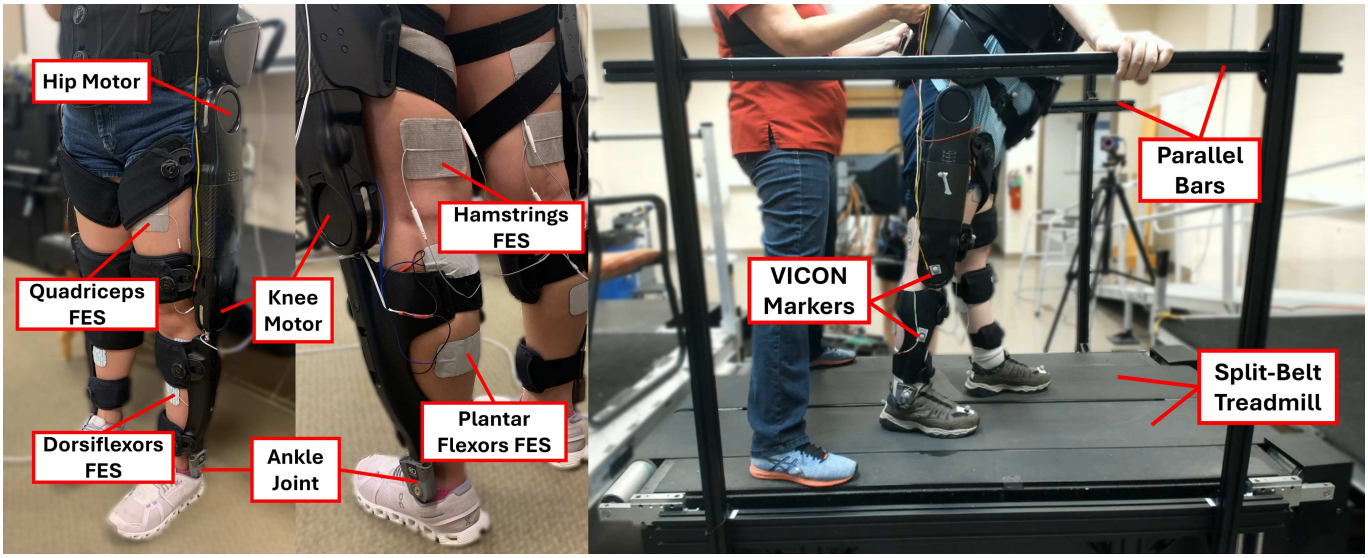

Fig. 10. a) Electrodes and Indego exoskeleton setup for the exoskeleton walking experiments. b) A participant with SCI on a treadmill during model identification and controller validation experiments.

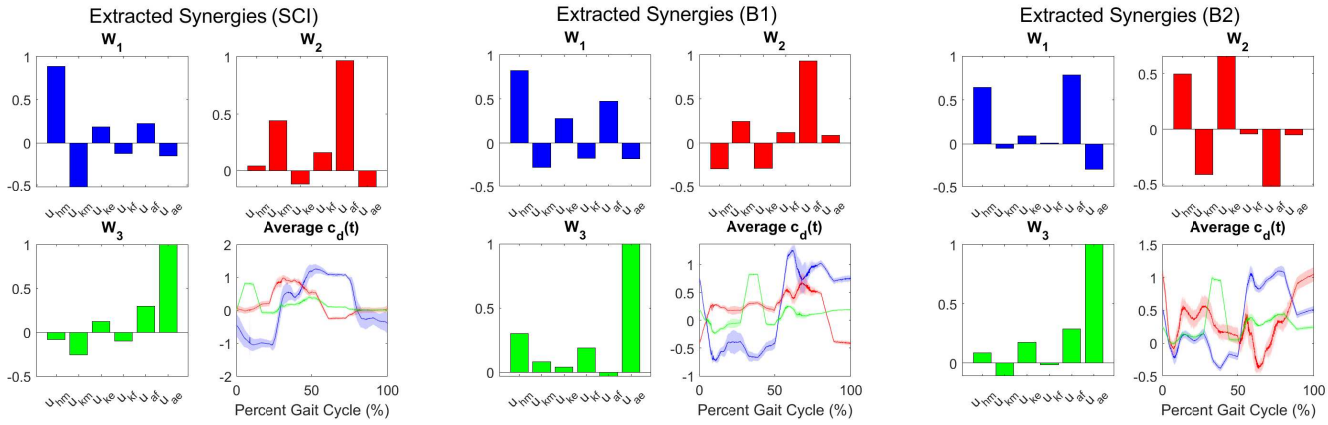

(a) (b) (c)

Fig. 11. Synergies extracted from walking data for (a) the participant with SCI, (b) participant B1, and (c) participant B2. W_1-W_3 are the time-invariant synergy weights. Corresponding average optimal activation trajectories $c_d(t)$ are presented to illustrate when each synergy is most active, but these were not used in subsequent control design.

for $u = [u_{hm}, u_{km}, u_{ke}, u_{kf}, u_{ae}, u_{af}]^T$, and the cost function in (18) is defined as

$$l\left(z(t|t_k), u(t|t_k)\right) = \|z - z_d\|_Q + \|u\|_R + \|\dot{u}\|_P,$$

for $Q \in \mathbb{R}^{\mathcal{H}\times\mathcal{H}}$, $R, P \in \mathbb{R}^{6\times 6}$.

3) **Synergistic MPC with Differently Penalized** c_1. In this case, the penalty weight in R corresponding to c_1 was changed to effect synergy redistribution. A greater penalty on c_1 should see a reduction in this activation signal, and vice versa.
4) **Synergistic MPC with Differently Penalized** c_3. In this case, the penalty weight in R corresponding to c_3 was changed to effect synergy redistribution.

VI. Exoskeleton-Assisted Walking Results

Total Execution Time

Total execution time (TET) was recorded for the duration of each walking trial using Simulink's Real-Time Task Execution Time Monitor. Results can be seen in Table IV. (Note that participants B1 and B2 did not participate in condition 3 and condition 4 experiments, respectively.) The synergistic case (condition 1) reduced computation time by over 28%, on average. This difference was found to be statistically significant ($p < 0.03$). When the penalties on c_1 or c_3 were changed compared to this baseline case, there was a similar reduction in computational cost.

A. *Effect of Penalizing Hip Flexion Synergy*

For participant B2 and participant S1, we changed the penalty on the first synergy (i.e., the penalty term in R in (17), corresponding to the first synergy's activation signal, was

Subject	TET (ms)			
	Synergies	No Synergies	Synergies (Different c_1 Penalty)	Synergies (Different c_3 Penalty)
B1	0.50	0.73	-	0.50
B2	0.68	0.82	0.65	-
SCI	0.53	0.82	0.53	0.53
Average $\pm$ SD	0.57 $\pm$ 0.08	0.79 $\pm$ 0.04	0.60 $\pm$ 0.06	0.51 $\pm$ 0.02

TABLE IV
TETs FOR EACH REAL-TIME CONTROL CONDITION TESTED.

increased/decreased). In the first synergy, across participants, the hip motor was the dominant input. Therefore, we intended to modify the hip flexion behavior by modifying the penalty terms. Specific penalty values are provided in Figs. 12-13. A consequence of employing personalized models is that cost function penalties need to be heuristically determined among participants. In both participants, a greater penalty on the first synergy's activation signal resulted in greater peak hip flexion, as shown in Figs. 12(b) for participant B1 and 13(b) for participant S1. For both participants, greater peak hip extension also occurred with a smaller penalty, which is unsurprising given that this synergy acts in the negative direction during the stance phase and in the positive direction during the swing phase, thus facilitating both extension and flexion. The hip motor torques were therefore increased in magnitude for both the stance and swing phases, as seen in Figs. 12(c) and 13(c) and reported in Table V. For comprehensive synergy activation, joint angle, and control input plots for both subjects, the reader is directed to the Supplementary Material.

B. Effect of Penalizing Push Off Synergy

For participants B1 and S1, we increased the penalty on the third synergy activation signal. Plantar flexion dominates in the third synergy toward the end of the stance phase, as illustrated in Fig. 11. In both participants, the magnitude of c_3 decreased with the greater penalty, as seen in Figs. 14 and 15. We anticipated that the increased penalty would lead to a reduction in the amount of FES delivered to the plantar flexors during push off. Surprisingly, we observed a decrease of > 4mA in ankle flexors FES for participant S1. Otherwise, control redistribution appeared to be minimal, as outlined in Table VI, although there was a small increase in hip motor torque (< 3Nm) in both participants. For comprehensive synergy activation, joint angle, and control input plots for both subjects, the reader is directed to the Supplementary Material.

VII. DISCUSSION

Multi-joint MPC of hybrid exoskeletons is computationally burdensome and has therefore necessitated linearization to achieve real-time control. Artificial synergies offer a bio-inspired means to reduce input dimensionality, but the relation between the number of synergies employed and the controller's ability to compensate for FES-induced fatigue has not yet been explored. The goals of this study were (1) to establish that using synergies to reduce input dimensionality also reduces computational burden and (2) to investigate how input dimensionality reduction affects fatigue compensation strategy. For both gait phases, the computational burden was indeed reduced in simulation when synergies were employed. Furthermore,we found that employing a greater number of synergies than was necessary to complete the motion enabled more control effort redistribution in response to fatigue.

For the DSP, the mean number of iterations decreased when the dimensionality was halved and two synergies were used as the control inputs, and this number decreased further when only 1 synergy was applied. The inclusion of a second synergy permitted greater freedom of control input allocation, which was important for fatigue compensation. Meanwhile, the average value of the cost function was only marginally different with synergies than for the full-dimensional case.

For the SSP, the computational cost was lower with the use of synergies, but the objective function value was greater. This may be due to information loss as the SSP uses more than twice as many actuators as the DSP. Furthermore, it incorporates knee joint motion and involves a more complex movement (namely, hip and knee flexion followed by knee extension [25]).

Although not pictured here, we found that conflict between the optimized $c(t)$ and the full-dimensional input constraints led to a deterioration in performance. An initial set of synergies extracted from a slower step and with a lower control cost saw frequent input saturation during simulation which deteriorated performance, causing the foot to drag rather than taking a step. This was because while the MPC was selecting synergy activations it believed to be optimal, the corresponding inputs could not be realized. After adjusting the cost function and desired trajectory used in the initial optimization, we extracted a set of synergies which proved more conducive to avoiding input saturation.

Incorporating bounds on u in the synergistic MPC could be strictly enforced in two ways. The first is to add further constraints on the full-dimensional inputs, namely, $[Wc]_i \in \mathcal{U}$, $\forall i$, where $\mathcal{U}$ is the set of allowable full-dimensional controls, but this would defeat the purpose of reducing computational cost. The second way is to constrain $|c_i|$ such that the resulting inputs are guaranteed to be contained in $\mathcal{U}$, but this would require such conservative bounds on c that the task may not be achievable. Besides enforcing non-negativity of FES inputs, for the SSP, we tuned the bounds on c such that optimal inputs were already in $\mathcal{U}$ in almost all cases. Saturation was enforced for inputs which exceeded their bounds without significantly deteriorating performance.

Several of our previous works have explored artificial synergy-based control. The adaptive control schemes in [23]–[26] are indeed model-based approaches, and the adaptive controller can account for model uncertainty. While the resulting control will converge to the desired trajectory, this may require

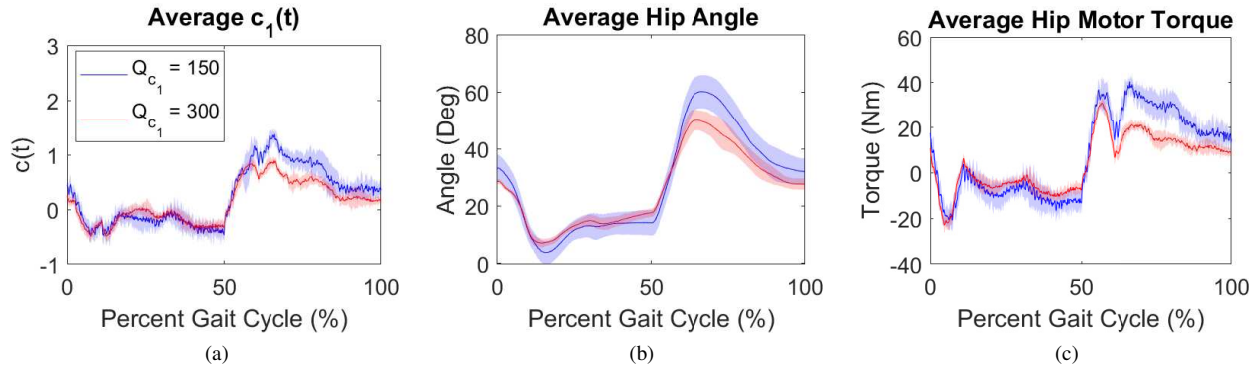

(a) (b) (c)

Fig. 12. (a) Average c_1 trajectories for different penalties on c_1 for participant B2. (b) Corresponding hip angle trajectories. (c) Corresponding hip motor trajectories.

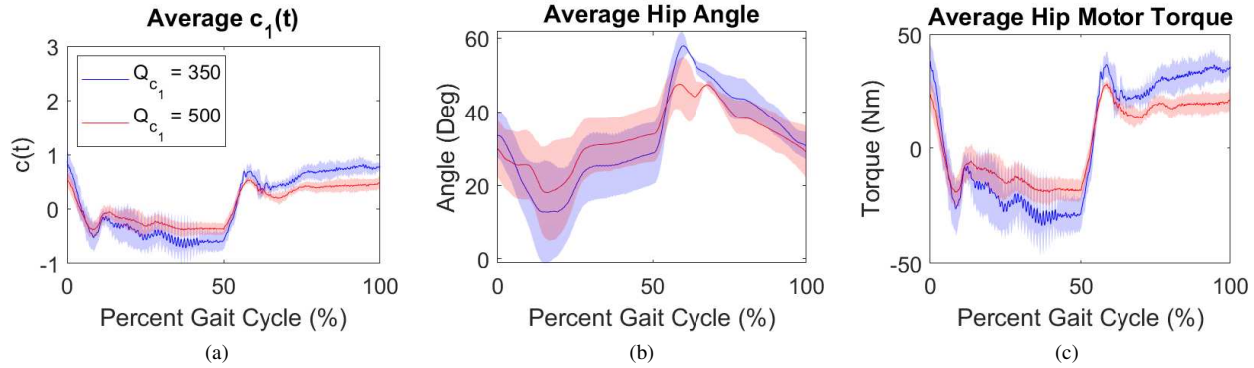

(a) (b) (c)

Fig. 13. (a) Average c_1 trajectories for different penalties on c_1 for participant S1. (b) Corresponding hip angle trajectories. (c) Corresponding hip motor trajectories.

Subject	Hip Motor (Nm)	Knee Motor (Nm)	Knee Extensors (mA)	Knee Flexors (mA)	Ankle Flexors (mA)	Ankle Extensors (mA)
S1	-10.15	-3.46	-1.67	-1.29	-0.05	-0.03
B2	-7.46	-0.15	-0.16	0.13	0.60	-1.63
Average	-8.81	-1.81	-0.92	-0.58	0.27	-0.83

TABLE V
CHANGE IN CONTROL INPUT RMS WITH HIGHER PENALTY ON c_1.

Subject	Hip Motor (Nm)	Knee Motor (Nm)	Knee Extensors (mA)	Knee Flexors (mA)	Ankle Flexors (mA)	Ankle Extensors (mA)
S1	2.27	-0.60	0.84	-0.08	-4.62	0.49
B1	2.52	0.03	0.76	1.27	0.68	0.29
Average	2.39	-0.28	0.80	0.59	-1.97	0.39

TABLE VI
CHANGE IN CONTROL INPUT RMS WITH HIGHER PENALTY ON c_3.

a large amount of control effort. Because optimal control distributes control effort between FES and motors based on a predefined cost function, the importance of trajectory tracking, control effort, muscle fatigue, etc. can be weighted to achieve the desired control performance. Furthermore, unlike adaptive control, the incorporation of state and control constraints is straightforward. Preliminary work in [36] presented a synergy-based MPC design in which the synergy activation signals were optimized. Although much more rigorous than the simple MPC scheme presented herein, the complexity of this MPC makes straightforward translation for real-time applications difficult. With the end goal of implementing synergy-based MPC, our simulations used a simplified control design that does not include the cascaded activation dynamics.

After identifying subject-specific linear models of exoskeleton walking and identifying personalized synergies, we leveraged MATLAB's mpcobj function to solve the optimal control problem in real-time. While this initial investigation modeled only one leg, incorporating both legs into a unified model and set of synergies would capture how each leg's motion affects the other, which is important when the task is to achieve a desired foot placement rather than follow time-dependent joint trajectories. Nonetheless, a pattern emerged among participants wherein 3 synergies account for $> 90\%$ of the variance; the most important synergy pertained to hip flexion during swing and extension during stance; and the

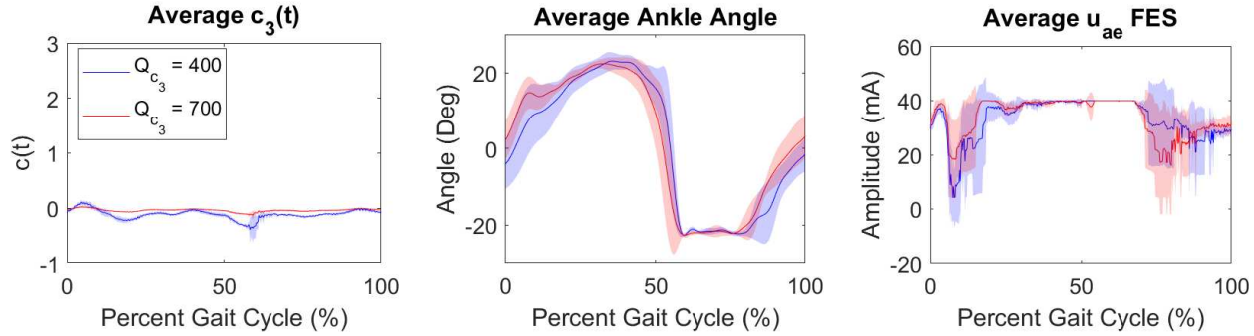

(a) (b) (c)

Fig. 14. (a) Average c_3 trajectories for different penalties on c_3 for participant B1. (b) Corresponding ankle angle trajectories. (c) Corresponding ankle extensors FES trajectories.

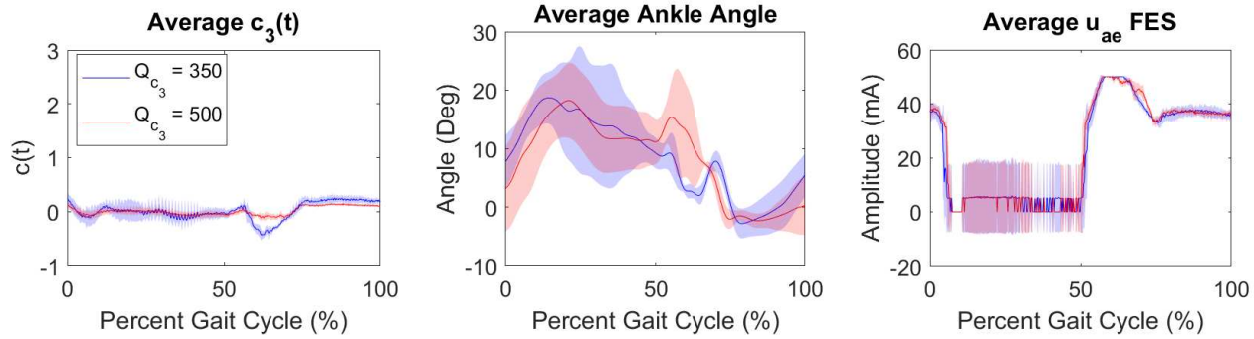

(a) (b) (c)

Fig. 15. (a) Average c_3 trajectories for different penalties on c_3 for participant S1. (b) Corresponding ankle angle trajectories. (c) Corresponding ankle extensors FES trajectories.

third most important synergy pertained to push off. Across participants, experimental results confirmed the simulation findings regarding computation time. Synergistic MPC significantly reduced computation time by $> 28\%$, and the loss of information did not cause a noticeable deterioration in walking performance (for video footage of synergistic and non-synergistic walking, see Supplementary File S1).

Also worth pointing out is that our previous work has seen success using only 2 synergies [23], [25]. These earlier approaches, however, incorporated robustifying feedback controllers that mitigated the information loss caused by truncating the number of synergies. For implementation purposes, it is desirable to incorporate such a feedback controller in order to further reduce input dimensionality and computational burden while improving trajectory tracking.

We found we could adjust controller behavior by modulating the cost function penalties on individual synergy activations. A lower penalty on the hip flexion/extension-dominant synergy activation signal resulted in greater hip motor torque and therefore more peak hip flexion/extension. A heavier penalty on the ankle extension-dominant synergy, however, did not result in reduced ankle extensor FES. Because each model and each set of synergies are person-specific, it could be that the penalty increase was insufficient to achieve the desired behavior, especially given that the magnitude of this synergy's activation was already quite small with the lower penalty. Alternatively, there could be inaccuracies in the data-driven model that result in a failure to capture the ankle joint response to FES.

We argue that, in a rehabilitation setting, penalizing synergies rather than individual inputs is more intuitive for therapists. If a patient needs more assistance with foot clearance, for example, the therapist could relax the penalty on a synergy dominated by the knee motor and ankle flexors. This is merely a preliminary study, and further investigation with more participants is needed in order to obtain a standardized method of tuning synergies across participants to achieve a desired walking pattern. Additionally, the fatigue reallocation benefits of including an extra synergy need to be tested in a real-world scenario.

The synergy analysis presented here is by no means exhaustive. We have investigated the computational benefits and control performance for slow, level-ground walking, but stair climbing, incline/decline walking, and even walking at different speeds require different muscle activations and would yield different synergy compositions. Nonetheless, based on our results, we propose cautious optimism as far as synergistic hybrid neuroprosthesis control is concerned. For a given application, the reduction in computational cost will have to be weighed against information loss and state prediction error due to unconstrained full-dimensional inputs. In our simulated case, 3 synergies were still able to complete the SSP task

even when the hip flexors were fully fatigued, highlighting the potential of this method.

This rehabilitative approach to synergies is distinct from the EMG-based approaches seen in works such as [22], [37]. Such methods use non-negative matrix factorization to extract EMG-derived muscle synergies from subjects with neurological disabilities such as stroke and, based on the EMG-derived synergies of subjects with no disabilities, formulate FES profiles designed to drive the impaired synergies toward more normative patterns. Several existing works even provide exoskeleton assistance based on the biological synergies of the user [38], [39]. Instead of EMG-based synergies, we employ *artificial* synergies, wherein the time-invariant weights represent FES and motor inputs rather than muscle activations. Artificial synergies are thus bio-inspired, but not biological. The benefit of artificial synergies is that they permit exoskeleton motors to be incorporated into synergy weight identification, which would be a non-trivial task with EMG-derived biological synergies. They can be identified through offline optimization, as was done in the simulations presented here, or, like EMG-based synergies, derived from actual hybrid exoskeleton walking data. We used a simple combination of PID and open-loop control during data collection, although other control methods could be used as well. In the future, person-specific hybrid exoskeleton models could be developed in OpenSim (Simbios, Stanford, CA, USA), and optimal, task-specific synergies could be extracted in the same manner we used for a simpler, four-link model simulation.

The person-specific linear models, while not the main emphasis of this work, are what enabled multi-joint synergistic MPC for real time, but they also pose their own limitations. Most notably, the cost function for each person had to be separately tuned to achieve smooth walking (that is, taking reasonably sized steps without chattering). Differences between person-specific models could also be why there was some variation in computation time. Participant B1, for example, had a TET of 0.50ms with synergistic MPC, while participant B2 had a TET of 0.68ms despite both participants using the same number of synergies.

VIII. Conclusion

Our work shows that bio-inspired artificial synergies significantly reduce the computational overhead of multi-joint MPC of hybrid exoskeletons. Using musculoskeletal gait models, we performed simulations with various numbers of synergies and with non-synergistic control, and we identified the resultant computational cost and fatigue compensation strategies. The use of synergies reduced the mean number of iterations per optimization step, regardless of initial muscle fatigue condition. Furthermore, for both gait phases, using the minimum number of synergies required to complete the task simply increased FES dosage to the fatigued muscle. A greater number of synergies had to be employed before control was reallocated to the exoskeleton motor inputs and away from the fatigued muscle. These findings suggest a tradeoff between computational cost reduction and fatigue compensation ability that should be considered in real-time synergistic MPCs for hybrid exoskeleton-based gait therapy. Our work also provides a practical approach to identify the nonlinear musculoskeletal walking dynamics from the experimental hybrid exoskeleton walking data and extract personalized synergies from a viable set of control inputs. Experiments with participants with and without SCI confirmed that the synergistic approach reduces MPC computation time when compared to a full-dimensional MPC. Furthermore, control reallocation can be achieved by altering the penalties on different synergy activation signals, providing an intuitive means of modulating gait assistance. Our approach opens a pathway to implement real-time optimal feedback approaches in gait assistance for people with neurological disorders, and these methods could be extended to other rehabilitation systems including upper-limb hybrid exoskeleton control. Future work will explore generalizable synergy activation tuning rules for obtaining different gait patterns and testing the reallocation strategies to compensate for the FES-induced fatigue in a larger SCI population.

Appendix

While this work addresses the computational cost incurred by using a large number of inputs during exoskeleton-assisted walking, there is another significant source of computational burden in MPC for multi-joint robots - the nonlinear dynamics. To address this, we implemented a data-driven model identification strategy, Extended Dynamic Mode Decomposition with Control [34], [35], which we previously explored in [40]. The approach identifies the nonlinear dynamics in (1) and (6) as a linear model in lifted space. The data-driven linear model eases the implementation of the optimal control problem in real time and bypasses tedious parameter identification process, as described in [41], for a multi-link limb model.

Let the original state consist of the angular joint positions and velocities of one leg, and let the control inputs consist of the normalized motor currents and FES inputs. The original state $x \in \mathbb{R}^6$ and control input $u \in \mathbb{R}^6$ are therefore given as

$$x = \left[q^T, \dot{q}^T\right]^T,$$
$$u = \left[u_{hm}, u_{km}, u_{ke}, u_{kf}, u_{ae}, u_{af}\right]^T.$$

We define a lifted state $z \in \mathbb{R}^{\mathcal{H}}$ as $z = \Psi := \left[\psi_1, \ldots, \psi_{\mathcal{H}}\right]^T$, where $\mathcal{H} > 6$ is the number of lifting functions $\psi(x)$. The first 6 lifting functions were simply the state x, but the remaining lifting functions, which were identified through trial and error for each individual, were trigonometric. By collecting $M+1$ lifted state and control data points and collecting them into $X_L, X_L^+ \in \mathbb{R}^{\mathcal{H}\times M}$, $U \in \mathbb{R}^{6\times M}$ as

$$X_L = \left[\Psi(x_1), \ldots, \Psi(x_M)\right],$$
$$X_L^+ = \left[\Psi(x_2), \ldots, \Psi(x_{M+1})\right],$$
$$U = \left[u_1, \ldots, u_M\right],$$

the dynamics can be approximated through simple linear algebra. Specifically, we can estimate the infinite-dimensional Koopman operator $\mathcal{K}$ as a finite-dimensional matrix $K^* \in \mathbb{R}^{\mathcal{H}\times(\mathcal{H}+6)}$ using the equation

$$K^* = X_L^+ \left[X_L, U\right]^\dagger.$$

The lifted state matrix $A \in \mathbb{R}^{\mathcal{H}\times\mathcal{H}}$ is simply the first $\mathcal{H}$ columns of K^*, with the remaining columns comprising the lifted control matrix $B \in \mathbb{R}^{\mathcal{H}\times 6}$. Through this method, the MPC from (13) was simplified as in (15) and (18).

For extracting synergies, we applied PCA to the data vector U consisting of PID and open-loop control inputs. For clarity, U may be expanded as

$$U = \begin{bmatrix} u_{hm}(t_1) & \dots & u_{hm}(t_M) \\ u_{km}(t_1) & \dots & u_{km}(t_M) \\ u_{ke}(t_1) & \dots & u_{ke}(t_M) \\ u_{kf}(t_1) & \dots & u_{kf}(t_M) \\ u_{ae}(t_1) & \dots & u_{ae}(t_M) \\ u_{af}(t_1) & \dots & u_{af}(t_M) \end{bmatrix}.$$

Since 3 synergies account for $> 90\%$ of the variance, the control data matrix may then be approximated as

$$U \approx \begin{bmatrix} W_1 & W_2 & W_3 \end{bmatrix} \begin{bmatrix} c_{d_1}(t_1) & \dots & c_{d_1}(t_M) \\ c_{d_2}(t_1) & \dots & c_{d_2}(t_M) \\ c_{d_3}(t_1) & \dots & c_{d_3}(t_M) \end{bmatrix}, \quad (19)$$

where each W_j, $j = [1, 2, 3]$, is a 6-element column vector.

REFERENCES

[1] C. Hartigan, C. Kandilakis, S. Dalley, M. Clausen, E. Wilson, S. Morrison, S. Etheridge, and R. Farris, "Mobility outcomes following five training sessions with a powered exoskeleton," *Topics in spinal cord injury rehabilitation*, vol. 21, no. 2, pp. 93–99, 2015.

[2] A. S. Khan, D. C. Livingstone, C. L. Hurd, J. Duchcherer, J. E. Misiaszek, M. A. Gorassini, P. J. Manns, and J. F. Yang, "Retraining walking over ground in a powered exoskeleton after spinal cord injury: a prospective cohort study to examine functional gains and neuroplasticity," *Journal of neuroengineering and rehabilitation*, vol. 16, pp. 1–17, 2019.

[3] T. Afzal, S.-C. Tseng, J. A. Lincoln, M. Kern, G. E. Francisco, and S.-H. Chang, "Exoskeleton-assisted gait training in persons with multiple sclerosis: a single-group pilot study," *Archives of physical medicine and rehabilitation*, vol. 101, no. 4, pp. 599–606, 2020.

[4] C. Bach Baunsgaard, U. Vig Nissen, A. Katrin Brust, A. Frotzler, C. Ribeill, Y.-B. Kalke, N. León, B. Gómez, K. Samuelsson, W. Antepohl *et al.*, "Gait training after spinal cord injury: safety, feasibility and gait function following 8 weeks of training with the exoskeletons from Ekso Bionics," *Spinal cord*, vol. 56, no. 2, pp. 106–116, 2018.

[5] A. J. Kozlowski, M. Fabian, D. Lad, and A. D. Delgado, "Feasibility and safety of a powered exoskeleton for assisted walking for persons with multiple sclerosis: a single-group preliminary study," *Archives of physical medicine and rehabilitation*, vol. 98, no. 7, pp. 1300–1307, 2017.

[6] N. Kapadia, K. Masani, B. Catharine Craven, L. M. Giangregorio, S. L. Hitzig, K. Richards, and M. R. Popovic, "A randomized trial of functional electrical stimulation for walking in incomplete spinal cord injury: effects on walking competency," *The journal of spinal cord medicine*, vol. 37, no. 5, pp. 511–524, 2014.

[7] R. Kobetic, R. J. Triolo, and E. B. Marsolais, "Muscle selection and walking performance of multichannel FES systems for ambulation in paraplegia," *IEEE Transactions on rehabilitation engineering*, vol. 5, no. 1, pp. 23–29, 1997.

[8] T. Street and C. Singleton, "A clinically meaningful training effect in walking speed using functional electrical stimulation for motor-incomplete spinal cord injury," *The Journal of Spinal Cord Medicine*, vol. 41, no. 3, pp. 361–366, 2018.

[9] A. Ekelem and M. Goldfarb, "Supplemental stimulation improves swing phase kinematics during exoskeleton assisted gait of SCI subjects with severe muscle spasticity," *Frontiers in neuroscience*, vol. 12, p. 374, 2018.

[10] A. J. Del-Ama, Á. Gil-Agudo, J. L. Pons, and J. C. Moreno, "Hybrid FES-robot cooperative control of ambulatory gait rehabilitation exoskeleton," *Journal of neuroengineering and rehabilitation*, vol. 11, no. 1, pp. 1–15, 2014.

[11] D. Zhang, Y. Ren, K. Gui, J. Jia, and W. Xu, "Cooperative control for a hybrid rehabilitation system combining functional electrical stimulation and robotic exoskeleton," *Frontiers in neuroscience*, vol. 11, p. 725, 2017.

[12] M. Nandor, R. Kobetic, M. Audu, R. Triolo, and R. Quinn, "A muscle-first, electromechanical hybrid gait restoration system in people with spinal cord injury," *Frontiers in Robotics and AI*, vol. 8, 2021.

[13] K. H. Ha, S. A. Murray, and M. Goldfarb, "An approach for the cooperative control of FES with a powered exoskeleton during level walking for persons with paraplegia," *IEEE Transactions on Neural Systems and Rehabilitation Engineering*, vol. 24, no. 4, pp. 455–466, 2015.

[14] N. Dunkelberger, J. Berning, E. M. Schearer, and M. K. O'Malley, "Hybrid FES-exoskeleton control: Using MPC to distribute actuation for elbow and wrist movements," *Frontiers in Neurorobotics*, vol. 17, p. 1127783, 2023.

[15] N. Dunkelberger, S. A. Carlson, J. Berning, E. M. Schearer, and M. K. O'Malley, "Multi degree of freedom hybrid FES and robotic control of the upper limb," *IEEE Transactions on Neural Systems and Rehabilitation Engineering*, 2024.

[16] T. Gold, A. Völz, and K. Graichen, "Model predictive interaction control for robotic manipulation tasks," *IEEE Transactions on Robotics*, vol. 39, no. 1, pp. 76–89, 2022.

[17] Z. Sun, A. Iyer, K. Lambeth, C. Cleveland, and N. Sharma, "Knee extension tracking and fatigue regulation results using a robust MPC approach in a hybrid exoskeleton," *Control Engineering Practice*, vol. 141, p. 105717, 2023.

[18] A. d'Avella, P. Saltiel, and E. Bizzi, "Combinations of muscle synergies in the construction of a natural motor behavior," *Nature neuroscience*, vol. 6, no. 3, pp. 300–308, 2003.

[19] M. C. Tresch and A. Jarc, "The case for and against muscle synergies," *Current opinion in neurobiology*, vol. 19, no. 6, pp. 601–607, 2009.

[20] F. M. Ramos, A. d'Avella, and M. Hayashibe, "Identification of time-varying and time-scalable synergies from continuous electromyographic patterns," *IEEE Robotics and Automation Letters*, vol. 4, no. 3, pp. 3053–3058, 2019.

[21] S. Ferrante, N. Chia Bejarano, E. Ambrosini, A. Nardone, A. M. Turcato, M. Monticone, G. Ferrigno, and A. Pedrocchi, "A personalized multi-channel FES controller based on muscle synergies to support gait rehabilitation after stroke," *Frontiers in neuroscience*, vol. 10, p. 425, 2016.

[22] J. Lim, T. Lim, J. Lee, J. Sim, H. Chang, B. Yoon, and H. Jung, "Patient-specific functional electrical stimulation strategy based on muscle synergy and walking posture analysis for gait rehabilitation of stroke patients," *Journal of International Medical Research*, vol. 49, no. 5, p. 03000605211016782, 2021.

[23] N. A. Alibeji, N. A. Kirsch, and N. Sharma, "A muscle synergy-inspired adaptive control scheme for a hybrid walking neuroprosthesis," *Frontiers in bioengineering and biotechnology*, vol. 3, p. 203, 2015.

[24] N. Alibeji, N. Kirsch, and N. Sharma, "An adaptive low-dimensional control to compensate for actuator redundancy and FES-induced muscle fatigue in a hybrid neuroprosthesis," *Control Engineering Practice*, vol. 59, pp. 204–219, 2017.

[25] N. A. Alibeji, V. Molazadeh, B. E. Dicianno, and N. Sharma, "A control scheme that uses dynamic postural synergies to coordinate a hybrid walking neuroprosthesis: Theory and experiments," *Frontiers in neuroscience*, vol. 12, p. 306806, 2018.

[26] N. A. Alibeji, V. Molazadeh, F. Moore-Clingenpeel, and N. Sharma, "A muscle synergy-inspired control design to coordinate functional electrical stimulation and a powered exoskeleton: artificial generation of synergies to reduce input dimensionality," *IEEE Control Systems Magazine*, vol. 38, no. 6, pp. 35–60, 2018.

[27] S. Dosen and D. B. Popovic, "Moving-window dynamic optimization: design of stimulation profiles for walking," *IEEE Transactions on Biomedical Engineering*, vol. 56, no. 5, pp. 1298–1309, 2009.

[28] N. Sharma, V. Mushahwar, and R. Stein, "Dynamic optimization of FES and orthosis-based walking using simple models," *IEEE Transactions on Neural Systems and Rehabilitation Engineering*, vol. 22, no. 1, pp. 114–126, 2013.

[29] D. Popovic, R. B. Stein, M. N. Oguztoreli, M. Lebiedowska, and S. Jonic, "Optimal control of walking with functional electrical stimulation: a computer simulation study," *IEEE Transactions on Rehabilitation Engineering*, vol. 7, no. 1, pp. 69–79, 1999.

[30] R. Riener, J. Quintern, and G. Schmidt, "Biomechanical model of the human knee evaluated by neuromuscular stimulation," *Journal of biomechanics*, vol. 29, no. 9, pp. 1157–1167, 1996.

[31] S. R. Goldberg, F. C. Anderson, M. G. Pandy, and S. L. Delp, "Muscles that influence knee flexion velocity in double support: implications for stiff-knee gait," *Journal of biomechanics*, vol. 37, no. 8, pp. 1189–1196, 2004.

[32] J. A. Andersson, J. Gillis, G. Horn, J. B. Rawlings, and M. Diehl, "CasADi: a software framework for nonlinear optimization and optimal control," *Mathematical Programming Computation*, vol. 11, pp. 1–36, 2019.

[33] D. A. Winter, *Biomechanics and motor control of human movement*. John wiley & sons, 2009.

[34] M. O. Williams, I. G. Kevrekidis, and C. W. Rowley, "A data–driven approximation of the koopman operator: Extending dynamic mode decomposition," *Journal of Nonlinear Science*, vol. 25, pp. 1307–1346, 2015.

[35] J. L. Proctor, S. L. Brunton, and J. N. Kutz, "Dynamic mode decomposition with control," *SIAM Journal on Applied Dynamical Systems*, vol. 15, no. 1, pp. 142–161, 2016.

[36] K. Lambeth, Z. Sun, M. Singh, and N. Sharma, "Robust MPC-based synergy control of a hybrid neuroprosthesis for foot placement," in *2022 IEEE Conference on Control Technology and Applications (CCTA)*. IEEE, 2022, pp. 1384–1389.

[37] C. M. Niu, Y. Bao, C. Zhuang, S. Li, T. Wang, L. Cui, Q. Xie, and N. Lan, "Synergy-based FES for post-stroke rehabilitation of upper-limb motor functions," *IEEE Transactions on Neural Systems and Rehabilitation Engineering*, vol. 27, no. 2, pp. 256–264, 2019.

[38] V. R. Garate, A. Parri, T. Yan, M. Munih, R. M. Lova, N. Vitiello, and R. Ronsse, "Walking assistance using artificial primitives: a novel bioinspired framework using motor primitives for locomotion assistance through a wearable cooperative exoskeleton," *IEEE Robotics & Automation Magazine*, vol. 23, no. 1, pp. 83–95, 2016.

[39] P. F. Nunes, I. Ostan, and A. A. Siqueira, "Evaluation of motor primitive-based adaptive control for lower limb exoskeletons," *Frontiers in Robotics and AI*, vol. 7, p. 575217, 2020.

[40] K. Lambeth, A. Iyer, and N. Sharma, "Quantifying functional electrical stimulation-induced fatigue via ultrasound for hybrid neuroprosthesis-based walking," in *2024 10th IEEE RAS/EMBS International Conference for Biomedical Robotics and Biomechatronics (BioRob)*. IEEE, 2024, pp. 1617–1622.

[41] N. Kirsch, N. Alibeji, and N. Sharma, "Nonlinear model predictive control of functional electrical stimulation," *Control Engineering Practice*, vol. 58, pp. 319–331, 2017.